

## Realization of an dimmable electronic ballast for a discharge lamps fed by an $L_sC_sC_p$ circuit and a PFC stage

Marref Mohammed Amine, Hamdaoui Habib, Seyf Eddine Bechekir

Intelligent Control and Electrical Power Systems (ICEPS) Laboratory, Department of Electrical Engineering, Djillali Liabes University, Sidi Bel Abbes, Algeria

### Article Info

#### Article history:

Received Sep 12, 2021

Revised Mar 22, 2022

Accepted Apr 8, 2022

#### Keywords:

Dimmable application

Discharge lamp

Electronic ballast

Electronic power

Power factor correction

### ABSTRACT

This paper presents an electronic ballast for discharge lamps. The ballast consists of two stages: i) a boost-buck chopper that performs the power factor correction and provides an approximately variable DC link voltage to drive the second stage and ii) a half-bridge MOSFET inverter with an improved series-parallel inductor-capacitor-inductor ( $L_sC_pL_p$ ) resonant circuit to drive the high-frequency discharge lamp. The electronic ballast designed here is a multi-purpose ballast which was experimentally tested for high-pressure sodium discharge lamps 150 W and metal halide lamps 150 W. It was revealed that this mode of operation makes it possible to vary and dim the light of the lamp and to improve the quality of the power supply while reducing the harmonic currents in networks.

This is an open access article under the [CC BY-SA](#) license.



### Corresponding Author:

Marref Mohammed Amine

Intelligent Control and Electrical Power Systems (ICEPS) Laboratory, Department of Electrical Engineering, Djillali Liabes University

Sidi Bel Abbes, Algeria

Email: sba89-9@hotmail.fr

## 1. INTRODUCTION

Today, street lighting, from the public electricity distribution network, represents around 15 to 20% of global energy consumption. It is important to note that more than 5% of the global gas emissions are greenhouse gases (GHGs). In addition, it is well known and widely admitted that the transition to new technologies would significantly reduce the consumption of energy to reach 939 TWh per year, which would consequently reduce CO<sub>2</sub> emissions by around 580 million tons per year [1]–[4].

For this reason, more efficient and economical lighting sources, such as light emitting diode (LED) lamps and gas discharge (GD) lamps have become increasingly popular because they represent a simple and inexpensive alternative solution for electricity consumption reduction [5]–[13]. Despite the good performance of LED lamps, which last longer and are more durable, and whose power can be easily increased, it was found that the gas discharge lamps are even more competitive, especially in applications that require high power because these lamps possess high energy efficiency. Moreover, no one denies the fact that low-wattage LED bulbs are more cost effective than high-wattage LED bulbs [14], [15].

Currently, several types of high-intensity discharge lamps are available on the market. The type of high-intensity discharge lamps that is widely spread on the market is the one that uses high pressure sodium (SHS) because of their high energy efficiency (lumen/watt) and their long life which can go up to 25000 hours with an acceptable color rendering index and a possibility of variation of their luminous flux or power (dimming) [16]–[20]. Based on all these advantages, it was decided to use, in the present work, a SHS lamp with 150 W power.

Over the past few years, high frequency electronic ballasts for gas discharge lamps have been touted as a replacement for magnetic ballasts due to their superior qualities and advantages such as their high efficiency (improved power factor), reduced weight, high luminous intensity, long lifespan, and possibility of controlling light intensity (dimming). For quite a few years now, varying the power of lamps has been a research topic of significant importance for a large number of researchers, because light intensity control through dimming can help to reduce energy consumption by around 40 to 60% [21]–[23]. It is widely acknowledged that the variation of the power of discharge lamps can be done in two different ways, namely through the variation of the frequency or else through the variation of the DC voltage applied at the input of the inverter. In recent past, a number of researchers [24], [25] have carried out a comparison between the two methods and found out that the second one is more advantageous as it allows having a more linear operation of the lamp.

Regarding high intensity discharge (HID) lamps, they are very complex systems. A complete model should include all the processes present in the gas discharge lamp, as well as the state variations of all chemical species. Several conductance models of discharge lamps have previously been proposed by some authors, [26]–[28]. However, many of these models were not established for the case of steady-state operation of the lamp. In fact, these models were not interested in the initiation phase or in the acoustic resonance phenomena. In this work, Figure 1 clearly shows that the resistance of the lamp could be considered as fitting a linear model on the large power scale [29], [30].

The present study aims to design and realize a class D (series–parallel) improved series–parallel inductor–capacitor–inductor ( $L_sC_pL_p$ ) electronic ballast that consists of two stages. The first stage comprises an AC/DC converter in series with a buck/boost converter that ensures the power factor correction (PFC). This stage is used to power our system as a resistive load and to provide a continuous link voltage that is slightly variable. The second stage consists of a half-bridge inverter with MOSFET switches and an  $L_sC_sC_p$  resonant circuit.

The remainder of this article is organized as shown in. The first part presents the electronic ballast. Next, the ignition procedure and lamp stability are described in part 2; then the design and realization of the electric system are discussed in part 3. Afterwards, the experimental results obtained, which show the feasibility of the proposed ballast, are presented in part 4. Finally, the fifth and last part draws conclusions and indicates opportunities for future research.

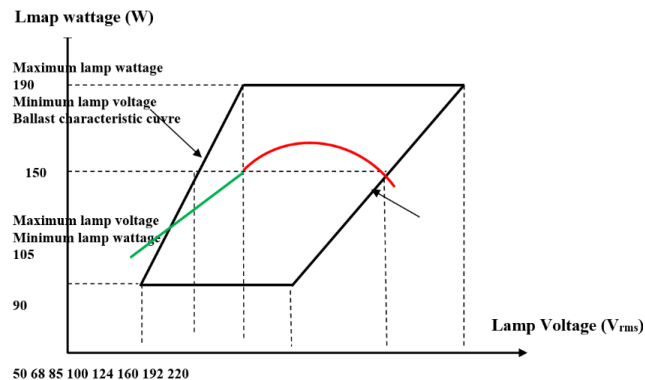


Figure 1. ANSI C78.42 operating limits for a 150-W-100-V<sub>rms</sub> HPS lamp [30]

## 2. STRUCTURES OF THE PROPOSED $L_sC_sC_p$ ELECTRONIC BALLAST

This type of electronic ballast enables a gas discharge lamp to be powered by a switch that is connected to a semiconductor circuit. It should be noted that the  $L_sC_sC_p$  (series–parallel) class D ballast filter of the lamp can be a low-pass filter in the start-up mode and a band-pass filter in the steady-state mode, depending on the resistance of the lamp. The ballast is supplied with a half-bridge inverter. This type of ballast is particularly used to power fluorescent lamps, as well as low and medium power discharge lamps.

The ballast architecture consists of two main stages. The first stage, which comprises a full-bridge rectifier in series with a boost chopper supplied with a command, which makes it possible to achieve the PFC, followed by a step-down DC/DC converter for the purpose of obtaining a direct voltage ( $V_{dc}$ ) within the interval [330–260] V to supply the second stage. Then, the second stage comprises a half-bridge inverter and an  $L_sC_sC_p$  resonant circuit. It should be noted that this stage is highly essential for supplying the lamp with alternating current with a high frequency (163–368) kHz. Note also that the high-frequency power supply to

this type of lamp helps to have a more stable operation. In addition, the various passive components used in the different stages, i.e. ignition, heating, steady state, and dimming, are fairly small in size. Figure 2 and Figure 3 shows the diagram of the proposed ballast.

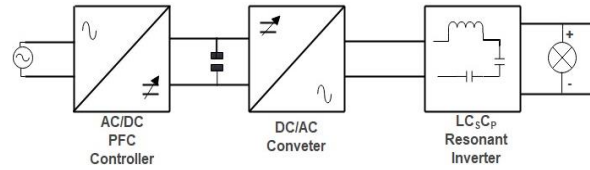


Figure 2. Block diagram of the electronic ballast proposed

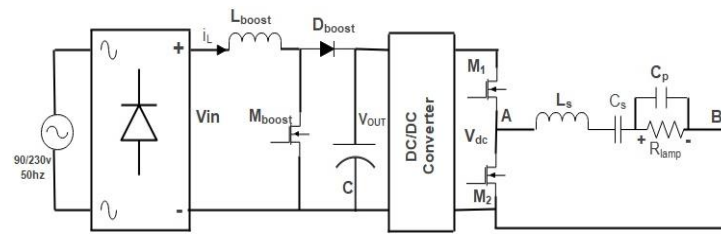


Figure 3. Two stage ballast block diagrams

## 2.1. Characteristics of the $L_sC_sC_p$ ballast

This section presents an  $L_sC_sC_p$  resonance circuit that is widely used in many applications. Due to the presence of a series capacitor ( $C_s$ ), the DC input voltage ( $V_{dc}$ ) is automatically blocked; in this case, the circuit can be supplied using a half-bridge inverter only. In the following sections, the characteristics of the  $L_sC_sC_p$  (series-parallel) class D ballast are presented in order to determine the passive components of the ballast. In addition, an electronic  $L_sC_sC_p$  ballast powered by an inverter is presented in Figure 4 (a). Further, the equivalent electronic ballast diagram is shown in Figure 4 (b).

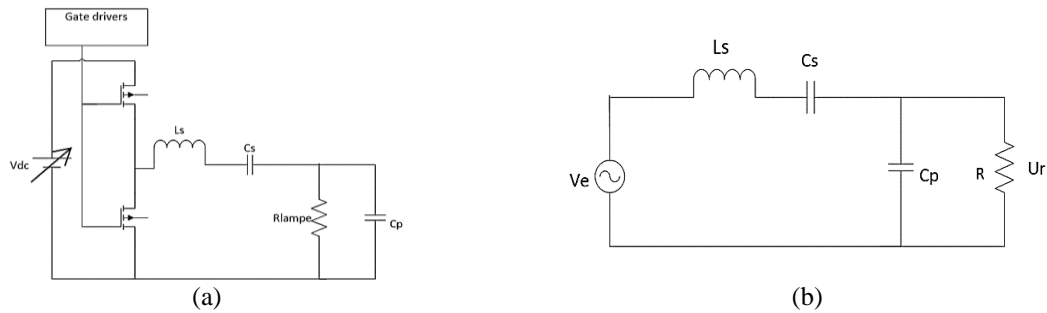


Figure 4. Diagram of the proposed ballast (a) class D  $L_sC_sC_p$  resonant inverter powered by inverter and (b) equivalent sinusoidal model

## 2.2. Electronic ballast transfer function

The equivalent sinusoidal model is shown in Figure 5. The electrical circuit is a voltage divider. The ratio of voltages is equal to the ratio of impedances.

$$G(p) = \frac{U_r}{V_e} = \frac{Z_p}{Z_s + Z_p} \quad p = j\omega \quad (1)$$

$$\begin{cases} Z_s = L_s * P + \frac{1}{C_s * P} \\ Z_p = \frac{R}{1 + R * C_p * P} \end{cases} \quad (2)$$

$$G(p) = \frac{U_r}{V_e} = \frac{RCsP}{1 + R(Cs + Cp)P + LsCsP^2 + RLsCsCpP^3} \quad (3)$$

### 2.3. Priming circuit

Before ignition, the lamp resistance is theoretically infinite. Now, the equivalent capacity  $C_{eq}$  of the two series capacitors  $C_s$  and  $C_p$  must be calculated as given (4).

$$C_{eq} = \frac{C_s * C_p}{C_s + C_p} \text{ si } C_s \gg C_p, C_{eq} \rightarrow C_p \quad (4)$$

It should be noted that our work should start only with the series inductor  $L_s$  and the parallel capacitor  $C_p$ . The ballast circuit in priming mode is presented in Figure 6. The ballast circuit in priming mode is then equivalent to a parallel  $LsCpR$  circuit which represents a low pass filter; it is described by a second-order differential equation.

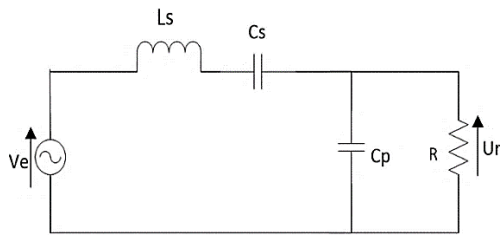


Figure 5. Equivalent electronic ballast diagram

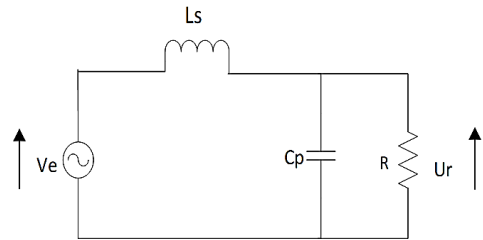


Figure 6. Equivalent diagram of priming in sinusoidal regime

#### 2.3.1. Circuit transfer function

The transfer function of the system can then be written in the form:

$$G(p) = \frac{U_r}{V_e} = \frac{1}{1 + \frac{Ls}{R}P + CpLsP^2} = \frac{K}{1 + \frac{2\xi}{\omega_p}P + \frac{1}{\omega_p^2}P^2} \quad (5)$$

Where:

$$\begin{cases} \xi = \sqrt{\frac{L}{C_p}} * \frac{1}{2R} : (\text{Amortization confiscations}) \\ \omega_p = \frac{1}{\sqrt{LsC_p}} : (\text{parallel natural pulsation}) \end{cases} \quad (6)$$

Therefore, the resonance pulsation can be written in the form:

$$\omega_r = \omega_p \sqrt{1 - 2\xi^2} = \frac{1}{\sqrt{LsC_p}} \sqrt{1 - \frac{Ls}{C_p R^2}} \quad (7)$$

It should be noted that before ignition, the resistance of the lamp can be considered as infinite:

$$R \rightarrow \infty, \omega_r \rightarrow \omega_p = \frac{1}{\sqrt{LsC_p}} \quad (8)$$

Note that it is possible to determine the priming pulsation as:  $\omega_p = \frac{1}{\sqrt{LsC_{eq}}}$ , with n capacity ratio  $C_s/C_p$ . In addition, it is also possible to write:

$$\omega_p = \frac{1}{\sqrt{LsC_s}} \sqrt{1 + n} = \omega_s \sqrt{1 + n} \quad (9)$$

Where:

$$\begin{cases} n = C_s/C_p : (\text{capacity report}) \\ \omega_s = \frac{1}{\sqrt{LsC_s}} : (\text{Serial pulse}) \end{cases} \quad (10)$$

### 2.3.2. Bode diagram of the system

Figure 7 makes it possible to see that on priming, the gain increases and takes very important values for the parallel resonance frequency  $f_p$ . Note that the voltage at the load is about 2 kV. This value is sufficient for the ignition of the system.

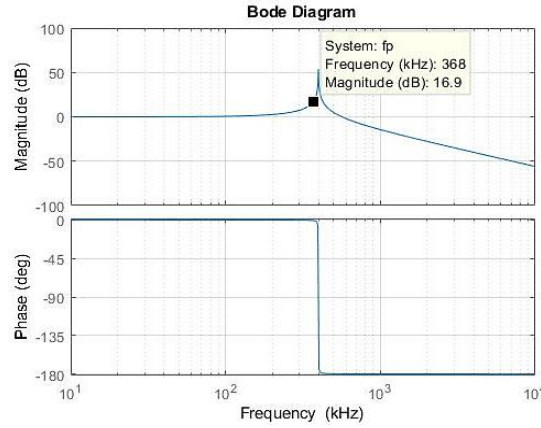


Figure 7. Bode diagram for the starting circuit

### 2.4. Steady state circuit

After ignition, the resistance of the lamp becomes much smaller than the impedance of the capacitor  $p$ , which implies that  $R \ll Z_{Cp}$  and  $Z_{eq}$  is between  $R$  and  $Z_{Cp}$  and tends towards 0. It is worth indicating that in steady state, the capacitor  $C_p$  can be overlooked, and only the inductance  $L_s$  and the capacitor  $C_s$  are taken into consideration. The ballast circuit in the steady state is presented in Figure 8. In the case of a SHP150 W lamp ( $R = 60 \Omega$ ) in the steady-state [8], one may write:

$$\begin{cases} Z_{cp} = \frac{1}{C_p \cdot p} : (\text{Impedance of capacitor } P) \\ Z_{eq} = \frac{R}{1 + R \cdot C_p \cdot p} : (\text{Equivalent impedance for } R \text{ and } C_p) \end{cases} \quad (11)$$

The ballast circuit in the steady state is then equivalent to a series  $RL_sCs$  circuit which represents a second-order band-pass filter. This type of filter makes it possible to filter out the frequencies that are outside its bandwidth.

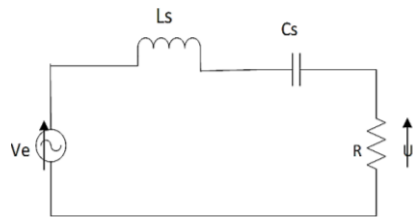


Figure 8. Equivalent steady-state ballast diagram

#### 2.4.1. Transfer function in this case

The transfer function of a second-order band-pass filter may be expressed in the form below:

$$G(p) = \frac{U_r}{V_e} = \frac{RC_s P}{1 + RC_s P + C_s L_s P^2} = \frac{1}{1 + (\frac{1}{Q_s}) * j(k - 1/k)}, p = j\omega \quad (12)$$

Where:

$$\begin{cases} K = \omega_s / \omega_0 : (\text{is the normalized pulsation}). \\ Q_s = R * \sqrt{\frac{C_s}{L_s}} : (\text{is the quality factor of the series circuit}). \end{cases} \quad (13)$$

Furthermore, the two cutoff frequencies are then given by:

$$\omega_{c1} = -\frac{R}{2Ls} + \sqrt{\left(\frac{R}{2Ls}\right)^2 + \left(\frac{1}{Lcs}\right)} \quad (14)$$

$$\omega_{c2} = \frac{R}{2Ls} + \sqrt{\left(\frac{R}{2Ls}\right)^2 + \left(\frac{1}{Lcs}\right)} \quad (15)$$

On the other hand, it is worth noting that the bandwidth  $\Delta\omega$  is equal to the difference between the two cutoff frequencies. Therefore:

$$\Delta\omega = \frac{R}{Ls} \quad (16)$$

Consequently, the optimum operating point as well as the quality factor  $Q_s$  of the series circuit can then be defined as the ratio of the bandwidth  $\Delta\omega$  over the series pulsation  $\omega_s$ . The bode diagram of the system in the steady state is presented in Figure 9.

$$Q_s = \frac{\Delta\omega}{\omega_s} \quad (17)$$

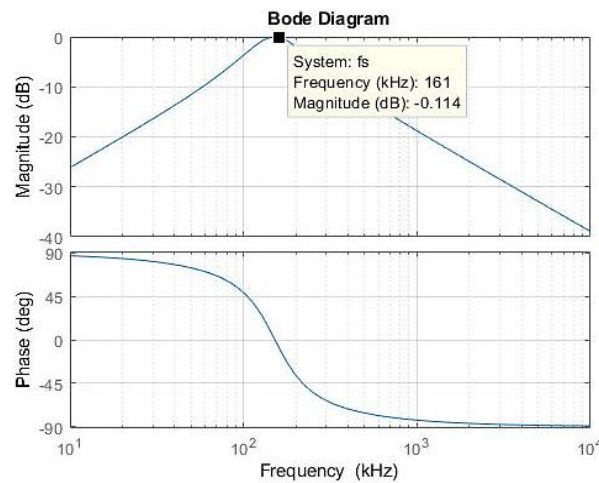


Figure 9. Bode diagram for the steady-state circuit

## 2.5. Modeling of an electronic ballast-discharge lamps

A model is generally defined as a mathematical tool that allows representing or faithfully reproducing a given real system. The model should not be too simple so as not to stray too far from the physical reality but, at the same time, it should not be too complex in order to simplify the analysis and synthesis of control structures. The objective of this work is to give an overview on the modeling of the electronic ballast for discharge lamps based on state equations that express the relationship between the various physical parameters that determine the state of the system, with a view to its steady state control. The equivalent sinusoidal model is shown in Figure 10.

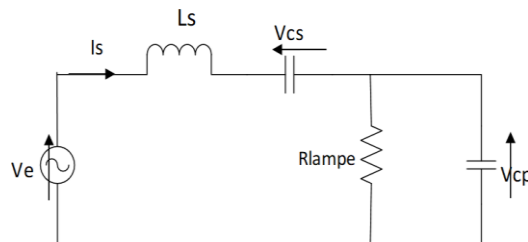


Figure 10. Equivalent model in sinusoidal regime

### 2.5.1. Mathematical model of the system

Based on the circuit given in the figure above, one may see that there are three state variables.  $I_s$ ,  $V_{cs}$  and  $V_{cp}$ .

$$\begin{cases} V_e(t) = L_s \frac{dis}{dt} + V_{cp}(t) + V_{cs}(t) \\ I_s(t) = C_s \frac{dV_{cs}}{dt} \\ I_s(t) = C_p \frac{dV_{cp}}{dt} + \frac{V_{cp}}{R} \end{cases} \quad (18)$$

$$\begin{cases} \frac{dis}{dt} = -\frac{1}{L_s} * V_{cp}(t) - \frac{1}{L_s} * V_{cs}(t) + \frac{1}{L_s} * V_e(t) \\ \frac{dV_{cs}}{dt} = \frac{1}{C_s} * I_s(t) \\ \frac{dV_{cp}}{dt} = \frac{1}{C_p} * I_s(t) - \frac{1}{R * C_p} * V_{cp}(t) \end{cases} \quad (19)$$

The system of differential equations can be written in the state space as follows:

$$\begin{pmatrix} \frac{dI_s}{dt} \\ \frac{dV_{cs}}{dt} \\ \frac{dV_{cp}}{dt} \end{pmatrix} = \begin{pmatrix} 0 & -\frac{1}{L_s} & -\frac{1}{L_s} \\ \frac{1}{C_s} & 0 & 0 \\ \frac{1}{C_p} & 0 & -\frac{1}{R * C_p} \end{pmatrix} \begin{pmatrix} I_s(t) \\ V_{cs}(t) \\ V_{cp}(t) \end{pmatrix} + \begin{pmatrix} \frac{1}{L_s} \\ 0 \\ 0 \end{pmatrix} V_e(t) \quad (20)$$

$$I_r = \begin{pmatrix} 0 & 0 & \frac{1}{R} \end{pmatrix} * \begin{pmatrix} I_s \\ V_{cs} \\ V_{cp} \end{pmatrix} \quad (21)$$

The above system of equations represents the mathematical model of the electronic ballast for discharge lamps of class D and type LCsCp (series-parallel). It can be represented on MATLAB Simulink MUX and FCN blocks in the Figure 11.

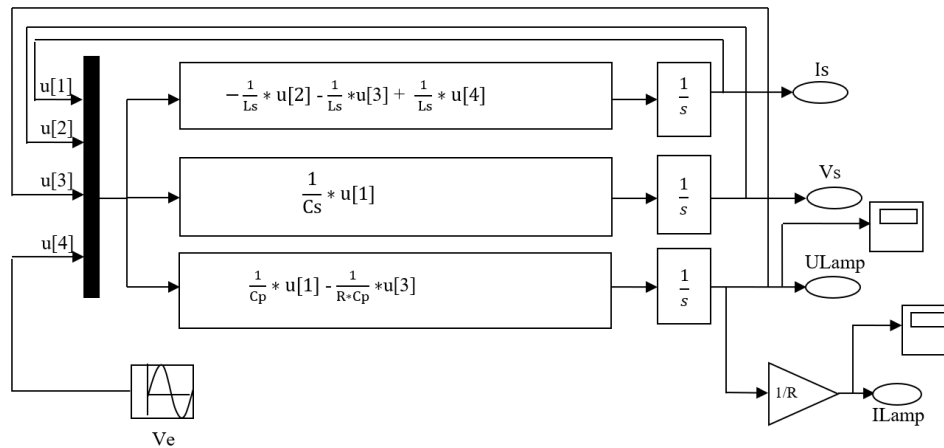


Figure 11. The model for the electronic ballast-lamps using the MATLAB/Simulink block

### 2.5.2. Simulation results

This static model allowed us, in spite of its simplicity, to validate quickly a certain number of hypotheses and experimental observations, in particular concerning what touches the gradation. It presents the advantage to be very easy to put in oeuvre and very flexible of use. Figure 12 shows the current and voltage curves at the lamp terminals, obtained from the model presented above. These curves adequately the experimental characteristics.



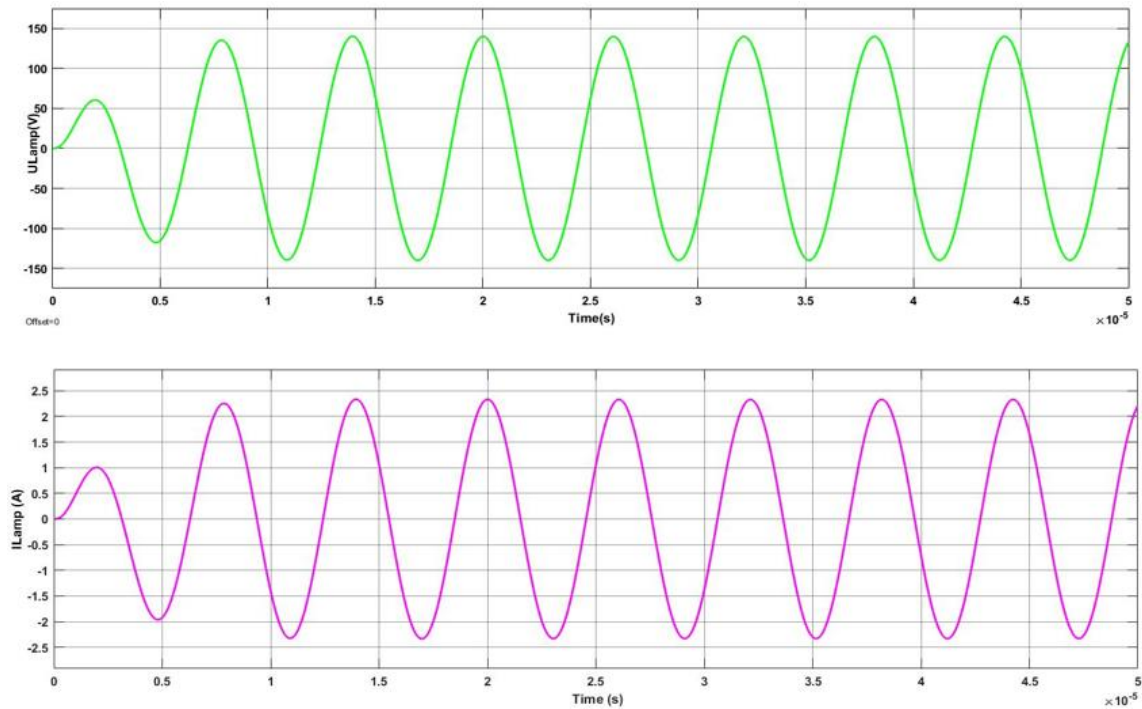


Figure 12. Current and voltage curve of the simulated ballast-lamp

## 2.6. Start-up lamp with circuit $L_s C_s C_p$

Figures 13 and 14 shows the frequency variation procedure for high-pressure sodium discharge lamp ignition with the LCsCp circuit as a function of time. According to Figure 7, it is quite possible to start the lamp with a frequency  $f_p$  equal to 368 kHz. In addition, it is useful to specify that the circuit was driven by a frequency close to the starting frequency  $f_p$  (point 1). Then, the frequency was gradually increased until the voltage ( $U_a$ ) at the terminals of the lamp reached a few Kilovolts. This voltage, which is sufficient to ignite the lamp, corresponds to point (2) [7], [8]. After that, the lamp, which is in the warm-up phase (point 3), changes its color. It should be noted that during this phase, the power supply frequency ( $f_s$ ) can be reduced to 161 kHz (point 4). Then the lamp takes a few minutes to reach its rated temperature and its rated speed.

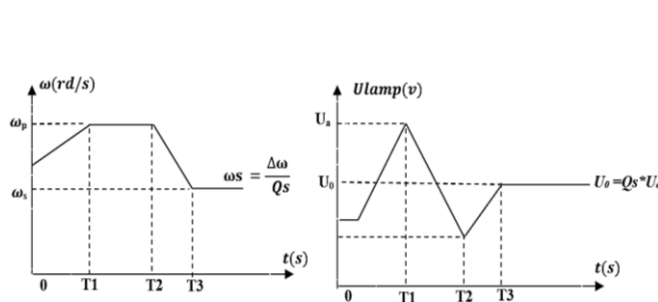


Figure 13. Shows the principle of start-up lamp as a function of time

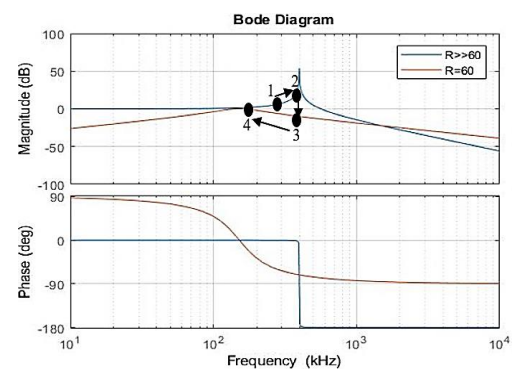


Figure 14. Presented the principle of start-up lamp by the bode diagram

## 2.7. Selecting the ballast parameters

In the steady state, the resistance of the lamp is well known, i.e.  $R=60 \Omega$ . In the present case, the lamp used is a 150 Watt high pressure sodium (SHF lamp). It is therefore possible to find the voltage at the resistance terminals. This voltage is equal to the series quality factor multiplied by the supply voltage  $U_e$ . Therefore,  $U_r = Q_s * U_e$ . Where:



$$Q_s = R \sqrt{\frac{C_s}{L_s}} : (\text{is the series quality factor}) \quad (22)$$

From Figure 1: on the other hand, the relation:  $P_{\text{lampe}} = U_{\text{eff}} \cdot i_{\text{eff}}$  used to calculate the rms value of the current:

$$i_{\text{eff}} = 1.5 \text{ A} \quad (23)$$

It is also possible to write  $P_{\text{lampe}} = R \cdot i_{\text{eff}}^2$ :

$$R = 60 \text{ ohm} \quad (24)$$

The voltage applied to the lamp is sinusoidal; its amplitude is expressed as:

$$U_r = \sqrt{2} \cdot U_{\text{eff}} = 141.4 \text{ V} \quad (25)$$

With regard to the amplitude of the supply voltage  $V_e$ , it was decided to take the fundamental harmonic value that is given by:

$$V_e = \frac{4 \cdot (V_{\text{dc}}/2)}{\pi} = 210.1 \text{ V} \quad (26)$$

Furthermore, the series quality factor is then expressed as:

$$Q_s = \frac{\Delta \omega}{\omega_s} = \frac{U_r}{U_e} = 0.67 < 0.707 \quad (27)$$

Therefore, considering  $Q_s$  and  $\omega_s = 2\pi \cdot f_s$ , it becomes possible to choose the parameters of the series resonance circuit such that:

$$Z_s = L_s \cdot \omega_s = \frac{1}{C_s \cdot \omega_s} \rightarrow Z_s = \frac{R}{Q_s} \quad (28)$$

$$L_s = \frac{R}{\omega_s \cdot Q_s} \text{ and } C_s = \frac{Q_s}{\omega_s \cdot R} \quad (29)$$

Finally, the choice of capacitor  $C_p$  was made by considering the capacitance ratio  $n = C_s/C_p$ . For a parallel frequency  $f_p$ , sufficient to create the ignition, the parallel pulsation can then be written as:

$$\omega_p = \frac{1}{\sqrt{L_s C_s}} \sqrt{1 + n} \quad (30)$$

## 2.8. Ballast parameters

The LCsCp filter sizing principle, in this case,  $L_s$  and  $C_s$  can be chosen for steady state operation of the ballast, imposing  $Q_s$  and  $\omega_s$ , the serial quality coefficient  $Q_s$  should be chosen to minimize the voltage gain attenuation and keep the linear phase region large enough to maintain the output signal quality of the LCsCp filter. Finally, we only need to define the parallel resonance frequency using equation 30 by imposing  $n$ , which represents the difference between the start frequency  $\omega_a$  and the series frequency  $\omega_s$ . The calculated practical values used in the prototype were: the series capacitor  $C_s = 11 \text{ nF}$ , the parallel capacitor  $C_p = 2.2 \text{ nF}$ , the value of the series inductance  $L_s = 88.5 \text{ }\mu\text{H}$ , the calculated series quality factor is  $Q_s = 0.67$ , and the DC voltage  $V_{\text{dc}} = 330 \text{ V}$ , the supply frequency in permanent mode is fixed  $\omega_s = 2\pi \cdot 161000 \text{ rd}$ , and therefore  $\omega_p = 2.36 \cdot 2\pi \cdot 161000 \text{ rd/s}$ .

## 3. REALIZATION

Figure 15 gives a clear representation of the overall functional plan of our study. It consists of an Arduino Uno microcontroller board, a control interface which includes the IR2113 driver circuit, in addition to the measuring devices, the ballast assembly which incorporates the half-bridge inverter and the LCsCp circuit that is powered by a variable DC voltage source, and which powers a lamp high pressure sodium (HPS) bulb 150 W.

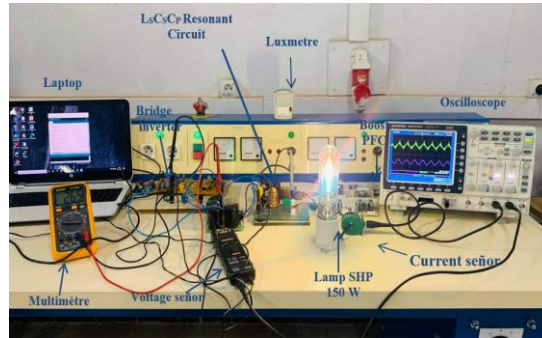


Figure 15. Photo of the proposed prototype

### 3.1. Construction of the second stage of the circuit

Figure 16 shows the architecture of the second stage of the circuit which includes a half-bridge inverter with two MOSFETs (30N60). The two switches are driven by the IR2113 driver with resistors, and a fast diode, a 10 ohm grid with a UF4007 diode in parallel. In addition, a 1 k $\Omega$  resistor and a 15 V Zener diode are placed in parallel for protection between the ground and the grid. Regarding the passive components of the resonant circuit, the series inductor used has a value  $L_s=90 \mu\text{H}$ ; the capacitors used have capacitance values  $C_s=13 \text{ nF}/1600 \text{ V}$  and  $C_p=2.2 \text{ nF}/2000 \text{ V}$ . The lamp used is a 150 W GE Lucalox HPS bulb.

In the present configuration, a program was developed for the purpose of generating a square signal, with a fixed ratio of 0.5. The inverter control uses a square wave control signal for the ignition of the system; its frequency is between 300 kHz and 368 kHz. Note that it uses the frequency sweep mode. In addition, the signal switching is performed using an Arduino electronic control board. The principle of frequency sweep is shown in Figures 10 and 11. The frequency is gradually lowered until the value  $f_s=163 \text{ kHz}$  is reached. The second control signal is then inverted using a 74ahc04 logic circuit, with a delay time between the two signals. This is achieved using a first-order low pass RC filter, with a delay time equal to  $0.1 \mu\text{s}$ . The two control signals are sent to an optocoupler which provides galvanic isolation between the control circuit and power circuit. In the present work, the HCPL2630 optocoupler was used. The control part is shown in Figure 17. The program used and presented in annexes.

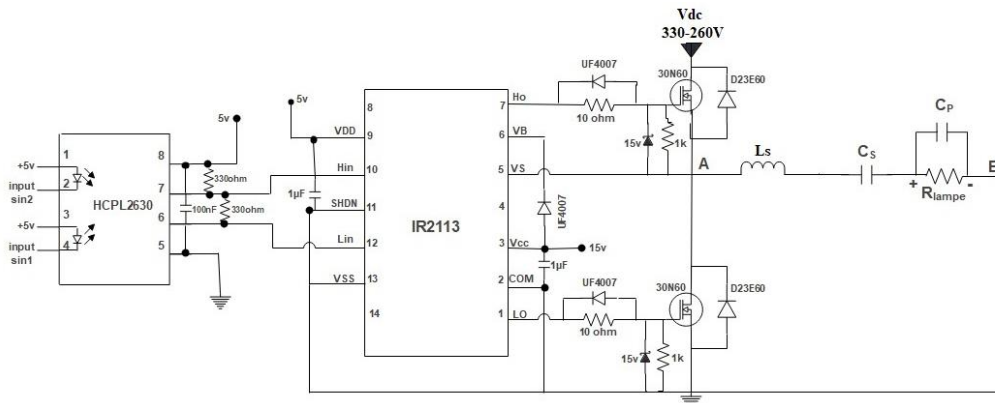


Figure 16. Power inverter diagram

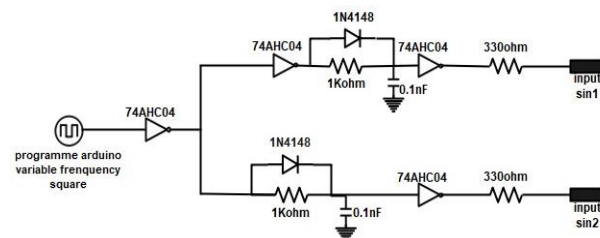


Figure 17. The inverter control diagram

#### 4. EXPERIMENTAL RESULT

A prototype of a half-bridge inverter has been developed and results have been obtained, initially, some experiments have been carried out concerning the generated pulses. The Figure 18 actually verifies the correct supply of signals for a switching frequency of 163 kHz, the pulses generated by the output of the Arduino control board, are sent to the SN74AHC04 which inverts them and, in turn, supplies the optocoupler HCPL2631. Figure 18 verifies the correct operation of the MOSFET driver IR2113. It can be seen that compared to the amplitude of the pulse at the input of SN74AHC04 (5 V), the output pulse of IR2113 has been correctly amplified (14 V) in order to drive the gate of the MOSFETs. A Figure 19 shows the experimental waveform of the voltage and the current of a 150 W Lucalox HPS bulb, Figure 19(a) presented the voltage and current of the lamp in the starting phase, and the Figure 19(b) presented current voltage and power of the lamp in steady state.

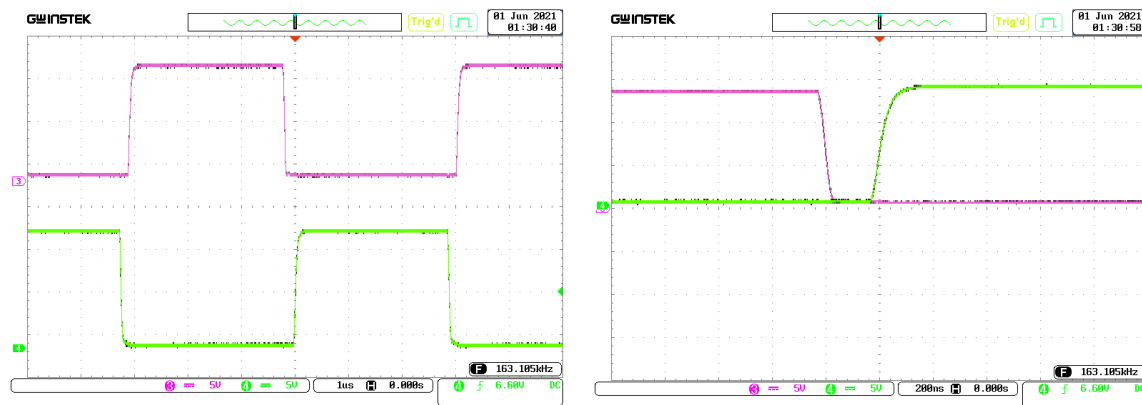


Figure 18. Control signal at output driver IR2113

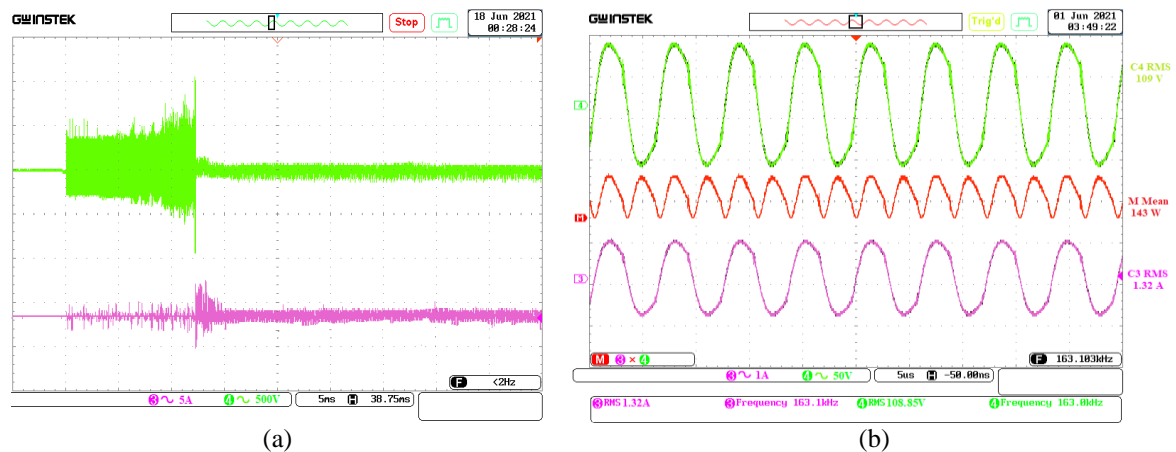


Figure 19. Shows the experimental results obtained for a lamp SHP 150 W: (a) voltage and current of the lamp in the starting phase and (b) current voltage and power of the lamp in steady state

##### 4.1. Power variation (dimming)

It is worth recalling that the main purpose of this work is to save energy. This part should therefore be considered as the most important part of our research. It mainly makes it possible to quantify the strong variations in the electrical and photometric quantities during operation at reduced power.

The present purpose is to reduce the power applied to the lamp. From this perspective, two fundamental alternatives are then possible. The first one consists in varying the frequency while the second involves varying the voltage  $V_{dc}$ . Moreover, it is useful to recall that in the steady state, the voltage value recorded at the load (resistance) is equal to the product of the series quality factor multiplied by the supply voltage. Therefore:

$$U_r = Q_s * U_e, \text{ with } Q_s = \Delta\omega/\omega_s.$$

Therefore, either the input voltage  $U_e$  must be increased or the series quality factor  $Q_s$  must be decreased, while varying the frequency. In the present case, it was decided to vary the direct voltage  $V_{dc}$ , which in turn automatically changes the power of the lamp. To do this, three power levels were defined: 143 W, 108 W, and 75 W. In order to allow for optimum stabilization of the thermodynamic equilibria of the plasma, a 3-minute minimum duration was chosen between the different power levels. The measured experimental result is presented in Figure 20, the Figure 20(a) 75% of the nominal power of the lamp, and the Figure 20(b) 50% of the nominal power of the lamp.

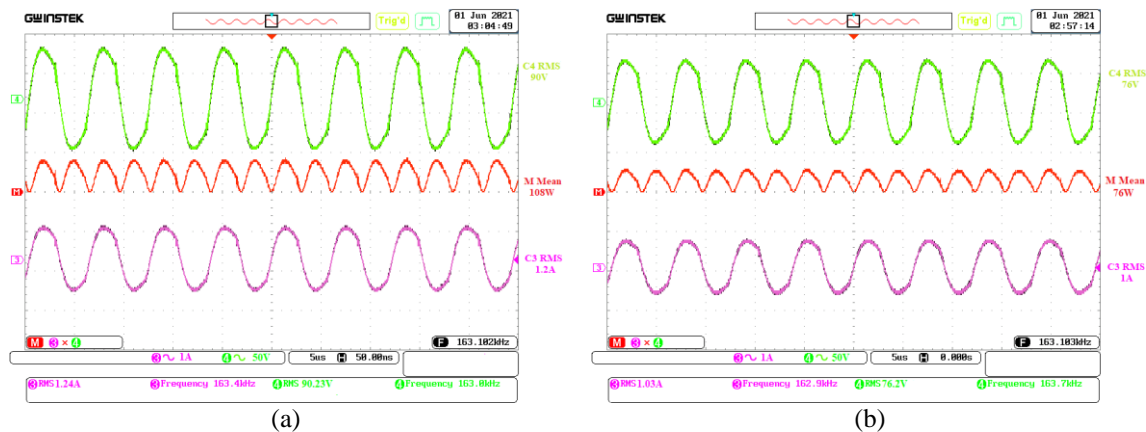


Figure 20. Voltage and current patterns for (a) 75% of the nominal power of the lamp and (b) 50% of the nominal power of the lamp

#### 4.2. Investigation of the total harmonic distortion and power factor correction of the input current

Analysis of the system under study indicates that the total harmonic distortion (THD) of the AC input power supply current was about 12% with a PFC stage. However, this THD was more than 96% in the absence of the PFC stage. These figures indicate that the power quality is quite good when the circuit is provided with a PFC stage. These results are good enough to meet the requirements of harmonic currents in networks. It is worth specifying that THD results were measured in the steady state. And the results of THD are shown in Figure 21, the Figure 21(a) with PFC stage, and the Figure 21(b) without PFC stage.

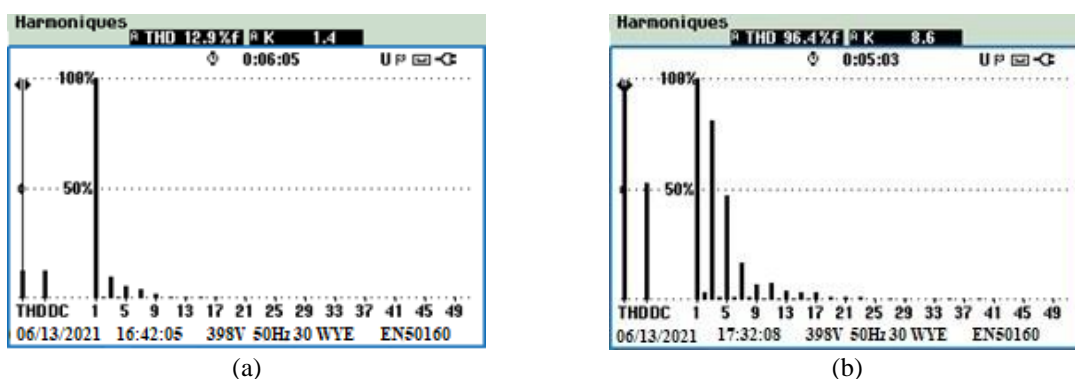


Figure 21. THD analysis of current AC with (a) PFC and (b) without PFC

### 5. CONCLUSION

This article focused on a two-stage electronic ballast provided with an  $L_sC_sC_p$  resonant circuit for powering discharge lamps using a power factor correction stage. It was found that the ballast delivers the desired power to the lamp regardless of the impedance of this lamp. This feature allows the lamp to operate at

rated wattage throughout its lifetime and makes it easy to vary the wattage of the lamp with more stable light dimming. Moreover, the ballast was tested with HPS lamps and metal halide (MH) lamps, with a power variation (dimming) between 100% and 50% of the nominal power of the lamp. Furthermore, the quality of the power supply was improved by adding a PFC stage. This made it possible to increase the power factor and reduce the harmonic currents from 96% to 12%, with a power factor close to unity. The findings of this work open new perspectives for future research. Indeed, it would be highly desirable to extend this research work through the examination of closed-loop regulation of the root mean square (RMS) lamp current in order to ensure the stability of the discharge current. In this case, two types of correction can be used. The first type concerns the classic PI correction and the second is the advanced adaptive correction. Then the two correction types should be compared.





## REFERENCES

- [1] H. V. Blavi, A. Leon-Masich, C. Olalla, and A. Cid-Pastor, "A Loss-Free Resistor-Based Versatile Ballast for Discharge Lamps," *Energies*, vol. 12, no. 7, p. 1403, Apr. 2019, doi: 10.3390/en12071403.
- [2] "The Street Lighting Market | Germany," (in France: Le Marché De L'éclairage Public | Allemagne), November 2021. [Online]. Available: <https://www.businesscoot.com/fr/etude/le-marche-de-leclairage-public-allemande>. (Date Accessed: Dec. 08, 2020).
- [3] "UN environnement programme," [Online]. Available: <https://wedocs.unep.org/search-filter?field=subject&filterorder=COUNT> 2019.
- [4] "Ecological Transition Agency," (in France: Agence de la transition écologique), [Online]. Available: [https://www.ademe.fr/sites/default/files/assets/documents/74511\\_7038\\_72dpi\\_eclairerjuste.pdf](https://www.ademe.fr/sites/default/files/assets/documents/74511_7038_72dpi_eclairerjuste.pdf).
- [5] Philips QL Induction Lighting Systems Information for Original Equipment Manufacturers, pp. 1-40, July 2007. [Online]. Available: [http://www.stefanslichtparade.de/files/ql\\_oem\\_guide.pdf](http://www.stefanslichtparade.de/files/ql_oem_guide.pdf).
- [6] P. Tabaka and P. Rozga, "Influence of a Light Source Installed in a Luminaire of Opal Sphere Type on the Effect of Light Pollution," *Energies*, vol. 13, no. 2, p. 306, Jan. 2020, doi: 10.3390/en13020306.
- [7] F. Giezendanner, J. Biela, and J. W. Kolar, "Optimization and Performance Evaluation of an AC-Chopper Ballast for HPS Lamps," in *IEEE Transactions on Industrial Electronics*, vol. 61, no. 5, pp. 2236–2243, May 2014, doi: 10.1109/TIE.2013.2274411.
- [8] J. Sebastian, D. G. Lamar, M. M. Hernando, M. Rodriguez, and A. Fernandez, "Average Small-Signal Modelling of the Power Stage of Power Factor Correctors with a Fast Output–Voltage Feedback Loop," *2009 Twenty-Fourth Annual IEEE Applied Power Electronics Conference and Exposition*, 2009, pp. 998–1004, doi: 10.1109/APEC.2009.4802784.
- [9] M. F. da Silva, *et al.*, "Analysis and Design of a Single-Stage High-Power-Factor Dimmable Electronic Ballast for Electrodeless Fluorescent Lamp," in *IEEE Transactions on Industrial Electronics*, vol. 60, no. 8, pp. 3081–3091, Aug. 2013, doi: 10.1109/TIE.2012.2203774.
- [10] M. A. Z. A. Rashid, A. Ponniran, M. K. R. Noor, J. N. Jumadri, M. H. Yatim, and A. N. Kasiran, "Optimization of PFC cuk converter parameters design for minimization of THD and voltage ripple," *International Journal of Power Electronics and Drive System (IJPEDS)*, vol. 10, no. 1, pp. 514–521, Mar. 2019, doi: 10.11591/ijpeds.v10.i1.pp514-521.
- [11] P. Stumpf, A. Lőrincz, and I. Nagy, "Stability of digitally controlled PFC boost converter with auxiliary state vector," *2013 IEEE International Symposium on Industrial Electronics*, 2013, pp. 1–6, doi: 10.1109/ISIE.2013.6563861.
- [12] Y. Jang and M. M. Jovanovic, "Interleaved Boost Converter with Intrinsic Voltage-Doubler Characteristic for Universal-Line PFC Front End," in *IEEE Transactions on Power Electronics*, vol. 22, no. 4, pp. 1394–1401, Jul. 2007, doi: 10.1109/TPEL.2007.900502.
- [13] A. Gil-de-Castro, A. Moreno-Munoz, J. J. G. de la Rosa, J. M. F. Arias, and V. Pallares-Lopez, "Study of harmonic generated by electromagnetic and electronic ballast used in street lighting," *2011 IEEE International Symposium on Industrial Electronics*, 2011, pp. 425–430, doi: 10.1109/ISIE.2011.5984196.
- [14] R. Stevenson, "The LEDs Dark secret: solid-state lighting won't supplant the light bulb until it can overcome the mysterious malady known droop," *IEEE spectrum*, August 2009.
- [15] A. Djuretic and M. Kostic, "Actual energy savings when replacing high-pressure sodium with LED luminaires in street lighting," *Energy*, vol. 157, pp. 367–378, Aug. 2018, doi: 10.1016/j.energy.2018.05.179.
- [16] L. Chhun, P. Maussion, S. Bhosle, and G. Zissis, "Characterization of Acoustic Resonance in a High-Pressure Sodium Lamp," in *IEEE Transactions on Industry Applications*, vol. 47, no. 2, pp. 1071–1076, Mar.–Apr. 2011, doi: 10.1109/TIA.2010.2102993.
- [17] M. A. D. Costa, A. L. Kirsten, J. M. Alonso, J. Garcia, and D. Gacio, "Analysis, Design, and Experimentation of a Closed-Loop Metal Halide Lamp Electronic Ballast," in *IEEE Transactions on Industry Applications*, vol. 48, no. 1, pp. 28–36, Jan.–Feb. 2012, doi: 10.1109/TIA.2011.2175681.
- [18] T. B. Marchesan, M. A. Dalla-Costa, J. M. Alonso, and R. N. do Prado, "Integrated Zeta–Flyback Electronic Ballast to Supply High-Intensity Discharge Lamps," in *IEEE Transactions on Industrial Electronics*, vol. 54, no. 5, pp. 2918–2921, Oct. 2007, doi: 10.1109/TIE.2007.899937.
- [19] R. Sikora and P. Markiewicz, "Assessment of Colorimetric Parameters for HPS Lamp with Electromagnetic Control Gear and Electronic Ballast," *Energies*, vol. 13, no. 11, p. 2909, Jun. 2020, doi: 10.3390/en13112909.
- [20] M. N. Nehdi, W. Nsibi, A. Chammam, A. Sellami, and G. Zissis, "Harmonic characterization of HPS lamp fed by two supply modes," *2015 7th International Conference on Modelling, Identification and Control (ICMIC)*, 2015, pp. 1–3, doi: 10.1109/ICMIC.2015.7409420.
- [21] T. Jang, H. Kim, and H. Kim, "Dimming Control Characteristics of Electrodeless Fluorescent Lamps," in *IEEE Transactions on Industrial Electronics*, vol. 56, no. 1, pp. 93–100, Jan. 2009, doi: 10.1109/TIE.2008.2009577.
- [22] S. Peters, M. Kettlitz, H. Schneidenbach, M. Wendt, and A. Kloss, "Dimming Characteristics of Metal-Halide Plasma Lamps," in *IEEE Transactions on Plasma Science*, vol. 36, no. 4, pp. 1178–1179, Aug. 2008, doi: 10.1109/TPS.2008.920904.
- [23] J. Zhou, F. Tao, F. C. Y. Lee, N. Onichi, and M. Okawa, "High power density electronic ballast for HID lamp," *Conference Record-IAS Annual Meeting IEEE Industry Applications Society*, vol. 3, pp. 1875–1880, Feb. 2002, doi: 10.1109/IAS.2002.1043789.
- [24] D. Y. Qiu, S. Y. Hui, and H. Shu-Hung Chung, "Parameter monitoring of high-frequency electronically operated discharge lamp systems," in *IEEE Transactions on Power Electronics*, vol. 20, no. 4, pp. 948–952, Jul. 2005, doi: 10.1109/TPEL.2005.850973.





- [25] J. Fraytag, *et al.*, "A Comparative Performance Investigation of Single-Stage Dimmable Electronic Ballasts for Electrodeless Fluorescent Lamp Applications," in *IEEE Transactions on Power Electronics*, vol. 30, no. 4, pp. 2239-2252, Apr. 2015, doi: 10.1109/TPEL.2014.2323591.
- [26] D. Buso, *et al.*, "Predictive Evaluation of Fluorescent Lamp Lifetime," *2009 IEEE Industry Applications Society Annual Meeting*, 2009, pp. 1-7, doi: 10.1109/IAS.2009.5324860.
- [27] M. Gulko and S. Ben-Yaakov, "Current-sourcing push-pull parallel-resonance inverter (CS-PPRI): theory and application as a fluorescent lamp driver," *Proceedings Eighth Annual Applied Power Electronics Conference and Exposition*, 1993, pp. 411-417, doi: 10.1109/APEC.1993.290693.
- [28] A. Gil-de-Castro, A. Moreno-Munoz, and J. J. G. de la Rosa, "Characterizing the harmonic attenuation effect of high-pressure sodium lamps," *Proceedings of 14<sup>th</sup> International Conference on Harmonics and Quality of Power-ICHQP 2010*, 2010, pp. 1-6, doi: 10.1109/ICHQP.2010.5625424.
- [29] C. Branas, F. J. Azcondo, and S. Bracho, "Design of LC/sub p/C/sub s/ resonant inverters as a power source for HID lamp ballast applications," in *IEEE Transactions on Industry Applications*, vol. 41, no. 6, pp. 1584-1593, Nov.-Dec. 2005, doi: 10.1109/TIA.2005.857468.
- [30] R. Casanueva, C. Branas, F. J. Azcondo, and S. Bracho, "Resonant converters: properties and applications for variable loads," *31<sup>st</sup> Annual Conference of IEEE Industrial Electronics Society, 2005. IECON 2005.*, 2005, p. 6, doi: 10.1109/IECON.2005.1569235.

## BIOGRAPHIES OF AUTHORS







**Marref Mohammed Amine**     was born in Sidi Bel-Abbes, Algeria, in 1990. researcher and doctoral student in 6<sup>th</sup> year, electrotechnics speciality machine control, at the intelligent control and electrical power systems (ICEPS) Laboratory in the Department of Electrical Engineering, Djillali Liabes University in the City of Sidi Bel-Abbes-Algeria. His current research focuses on power electronic converters and public lighting optimization. He can be contacted at email: sba89-9@hotmail.fr.



**Habib Hamdaoui**     was born in Sidi Bel-Abbes, Algeria, in 1970. He received the B.Sc., M.Sc., and Ph.D. degrees in electrical engineering from the University of Djilali Liabes, Sidi Bel-Abbes, in 1994, 1997 and 2004, respectively. Since 2021 he has been a professor of electrical engineering at the same university. His area of research includes power electronics, active power filter, electrical drives, and stability improvement by advanced FACTS devices. He can be contacted at email: hamdaoui\_h@outlook.fr.



**Seyf Eddine Bechekir**     was born in Bouira, Algeria, 1991. In 2021, he received a Doctorate degree from the University of Sidi Bel Abbes, in Electrical Engineering, where he is currently a professor tutor in the Department of Electrical Engineering. During 2015-2021, he joined in intelligent control and electrical power systems laboratory, University of Sidi Bel Abbes. His current research interests include the application of power electronics converts and plasma technology. He has published a lot of research papers in international journals and conference proceedings. He can be contacted at email: seyfeddine.electrotechnique@gmail.com.